

# Suitability of magnetic single- and multi-core nanoparticles to detect protein binding with dynamic magnetic measurement techniques



Hilke Remmer\*, Jan Dieckhoff, Meinhard Schilling, Frank Ludwig

Institute of Electrical Measurement and Fundamental Electrical Engineering, TU Braunschweig, Hans-Sommer-Str. 66, D-38106 Braunschweig, Germany

## ARTICLE INFO

### Article history:

Received 30 June 2014

Received in revised form

15 October 2014

Accepted 18 October 2014

Available online 22 October 2014

### Keywords:

Magnetic nanoparticles

Homogeneous bioassay

Dynamic magnetic measurements

## ABSTRACT

We investigated the binding of biotinylated proteins to various streptavidin functionalized magnetic nanoparticles with different dynamic magnetic measurement techniques to examine their potential for homogeneous bioassays. As particle systems, single-core nanoparticles with a nominal core diameter of 30 nm as well as multi-core nanoparticles with hydrodynamic sizes varying between nominally 60 nm and 100 nm were chosen. As experimental techniques, fluxgate magnetorelaxometry (MRX), complex ac susceptibility (ACS) and measurements of the phase lag between rotating field and sample magnetization are applied. MRX measurements are only suited for the detection of small analytes if the multivalency of functionalized nanoparticles and analytes causes cross-linking, thus forming larger aggregates. ACS measurements showed for all nanoparticle systems a shift of the imaginary part's maximum towards small frequencies. In rotating field measurements only the single-core nanoparticle systems with dominating Brownian mechanism exhibit an increase of the phase lag upon binding in the investigated frequency range. The coexistence of Brownian and Néel relaxation processes can cause a more complex phase lag change behavior, as demonstrated for multi-core nanoparticle systems.

© 2014 Elsevier B.V. All rights reserved.

## 1. Introduction

The realization of homogeneous binding assays utilizing specifically functionalized magnetic nanoparticles (MNPs) as markers has been demonstrated by a number of groups applying various techniques. The advantage of homogeneous bioassays is that a simple “mix-and-measure” principle can be realized, i.e., there are no washing steps of unbound markers required since they can be distinguished from the bound markers by their different relaxation time. The differentiation between bound and unbound markers is based on the fact that the conjugation of analytes to MNPs causes an increase of the MNP's hydrodynamic size. This is directly measurable as a change of the Brownian relaxation time, assuming that the Brownian rotation is the dominating mechanism. Consequently, homogeneous binding assays realized with any of the experimental techniques studied in this paper have the potential for a fast, sensitive and quantitative detection of proteins, such as cancer markers.

In a magnetorelaxometry (MRX) measurement, the MNP's magnetic moments are aligned by a magnetizing field and after abruptly switching off the magnetizing field, the decay of the sample's magnetic moments is measured as a function of time [1–4]. Alternatively,

in ac susceptibility (ACS) measurements, the MNPs are exposed to a sinusoidal field and a frequency sweep is performed. From the complex voltage induced in a gradiometric induction coil real and imaginary part of the ACS can be determined [5–7]. In order to avoid the time-consuming frequency sweep, the so-called susceptibility reduction technique was introduced [8,9]. Another experimental refinement to eliminate dia- or paramagnetic signals from the matrix was the application of the frequency mixing technique, utilizing the nonlinear magnetization-vs.-field curve of superparamagnetic nanoparticles [10–12]. In the comparably new rotating magnetic field technique (RMF), the MNPs are exposed to a rotating magnetic field and the phase lag between the rotating field and the sample magnetization is recorded [13,14].

In this paper, different magnetic nanoparticle systems are investigated regarding the change of the MNP dynamics caused by the conjugation of proteins which bind to the nanoparticle surface via the biotin-streptavidin complex. Especially, the difference between single- and multi-cores regarding the change of their dynamics is investigated. The nanoparticle response is measured and analyzed utilizing different dynamic magnetic measurement techniques: complex ac susceptibility, fluxgate magnetorelaxometry and the rotating magnetic field technique. As a non-magnetic reference technique, photon cross-correlation spectroscopy (PCCS) is applied.

\* Corresponding author.

E-mail address: [h.remmer@tu-bs.de](mailto:h.remmer@tu-bs.de) (H. Remmer).

## 2. Experimental

### 2.1. Materials

In this paper single-core and multi-core nanoparticles with iron oxide cores are investigated. The organic shell of all particle systems is functionalized with streptavidin. Streptavidin-biotin is one of the strongest covalent bindings and therefore it is an appropriate model binding system.

As single-core particle system, SHS-30 particles from Ocean NanoTech (Springdale, AR, USA) with a nominal core diameter of 30 nm were used. Three different multi-core particle systems were investigated: Strep SPIO – based on FeraSpin R – with a hydrodynamic diameter of 70 nm from nanoPET Pharma GmbH (Berlin, Germany) and BNF 80 as well as BNF 100 both synthetized by micromod Partikeltechnologie GmbH (Rostock, Germany) with a mean hydrodynamic diameter of 80 nm and 100 nm.

As an analyte biotinylated anti-human alpha-fetoprotein (AFP) purchased from ebioscience (Frankfurt, Germany) is applied. It has a molecular mass of 150 kDa and is coated with biotin.

In order to obtain a comparable coverage of the surface of the streptavidin functionalized nanoparticles with AFP analyte for all MNP systems, we choose a constant ratio between the nanoparticle mass concentration  $c(\text{MNP})$  multiplied by the nanoparticle surface  $\pi d_h^2$  – assuming that the density of streptavidin is about the same for all nanoparticle systems – and the analyte mass concentration  $c(\text{AFP})$ :

$$\frac{\pi d_h^2 c(\text{MNP})}{c(\text{AFP})} = 1.7 \times 10^{-16} \text{ m}^2 \quad (1)$$

The iron content is for all samples the same and amounts to 3.98 mM. Freeze-dried reference samples were compared with the corresponding suspended samples in order to estimate the fraction of particles in suspension that are dominated by the Brownian mechanism.

### 2.2. Experimental techniques

Magnetorelaxometry – either based on SQUIDs or on fluxgates as sensors – is a well-known technique to characterize magnetic nanoparticles. In our fluxgate-based MRX setup, the MNP's moments are aligned by a magnetizing field of 2 mT magnitude for 2 s. After abruptly switching off the magnetic field, the decay of the magnetic signal is recorded by a differential fluxgate setup. The magnetorelaxation signal of MNPs in solution with distributions of core  $f(d_c)$  and hydrodynamic size  $f(d_h)$  can be described by the cluster moment superposition model (CMSM) with the assumption of non-interacting nanoparticles [15,16]:

$$m_r(t) = \phi M_s \int_0^\infty f(d_h) \int_0^\infty f(d_c) \frac{\pi}{6} d_c^3 L(d_c) \times \left\{ 1 - \exp \left[ -\frac{t_{\text{mag}}}{\tau_{\text{eff},H}} \right] \right\} \exp \left[ -\frac{t}{\tau_{\text{eff}}} \right] dd_c dd_h \quad (2)$$

The factor  $\phi M_s$  accounts for the reduced saturation magnetization due to the low volume fraction of magnetic material. The Langevin function  $L(d_c)$  is given by

$$L(d_c) = \coth \left( \frac{\mu_0 M_s \pi d_c^3 H}{6k_B T} \right) - \frac{6k_B T}{\mu_0 M_s \pi d_c^3 H} \quad (3)$$

with the magnetic moment  $m = M_s \pi d_c^3 / 6$  assuming a spherical particle core shape. For the distribution of core and hydrodynamic diameter, lognormal functions are assumed.

In a MNP suspension, the relaxation can take place via the Brownian and the Néel mechanism with an effective time

constant:

$$\tau_{\text{eff}} = \frac{\tau_B \tau_N}{\tau_B + \tau_N} \quad (4)$$

with the Brownian time constant:

$$\tau_B = \frac{3\eta V_h}{k_B T} \quad (5)$$

and the Néel time constant:

$$\tau_N = \tau_0 \exp \left( \frac{K_{\text{eff}} V_c}{k_B T} \right). \quad (6)$$

The effective time constant  $\tau_{\text{eff},H}$  in (2) includes the Néel time constant in a static magnetic field; the utilized expression can be found in [17]. The Brownian time constant  $\tau_B$  depends on the solution's viscosity  $\eta$ , the particle hydrodynamic volume  $V_h$  and the thermal energy  $k_B T$ . The effective anisotropy constant  $K_{\text{eff}}$ , and the particle core volume  $V_c$  determine the Néel time constant  $\tau_N$ , for  $\tau_0$  a value of  $10^{-9}$  s is assumed. To restrict the number of free parameters for fitting measured MRX curves, the core parameters  $K_{\text{eff}}$  and  $V_c$  are independently obtained from a fit of the MRX curve measured on an immobilized reference sample. Since the MNP relaxation can only take place via the Néel mechanism, Eq. (2) simplifies to the MSM and the integration has only to be carried out via the core diameter.

In a measurement of the complex ac susceptibility, the MNP sample is exposed to a sinusoidal magnetic field and a frequency sweep is performed. Due to the comparably large hydrodynamic sizes of the multi-core particles, we utilize a fluxgate-based measurement system with a frequency range between 2 Hz and 9 kHz and a field amplitude of 200  $\mu$ T rather than our high-frequency 1 MHz ACS setup. In the fluxgate-based system, the sinusoidal magnetic field is generated by a Helmholtz coil and the induction signal is measured by two differentially aligned fluxgate sensors. The susceptibility spectra are fitted with a generalized Debye model [18,19], which takes into account the distributions of core  $f(d_c)$  and hydrodynamic diameters  $f(d_h)$ , the effective time constant  $\tau_{\text{eff}}$  and – as the CMSM for MRX – it neglects particle-particle interactions. The imaginary part of the ac susceptibility is given by [19]

$$\chi''(\omega) = \chi_0^* \int_0^\infty f(d_h) \int_0^\infty \frac{d_c^6 f(d_c) \omega \tau_{\text{eff}}}{1 + (\omega \tau_{\text{eff}})^2} dd_c dd_h \quad (7)$$

with

$$\chi_0^* = \frac{\mu_0 n M_s^2}{3k_B T} \left( \frac{\pi}{6} \right)^2 \quad (8)$$

Alternatively to applying a sinusoidal field along one direction, the MNPs can also be exposed to a rotating magnetic field. In a rotating magnetic field measurement, the phase lag between the rotating field and the MNPs magnetic moment direction is measured which is caused by viscous drag forces. The used RMF system works with a 2-axis Helmholtz coil system for the excitation and two differentially aligned fluxgate sensors for the detection of the MNP sample's stray field [20]. The frequency is swept between 20 Hz and 5 kHz with a magnetic field amplitude of 1 or 5 mT.

The phase lag  $\varphi$  between the rotating field and magnetization directions is given by

$$\varphi = \arctan \left( \frac{M''}{M'} \right) \quad (9)$$

with the real and imaginary parts  $M'$  and  $M''$  of the sample magnetization. The rotational dynamics of the MNPs' magnetization in the nonlinear range can be described by the Fokker-Planck

equation [21]. Accounting for distributions of core  $f(d_c)$  and hydrodynamic diameters  $f(d_h)$ , the normalized real and imaginary parts of the flux density  $B'_s(H, \omega)$  and  $B''_s(H, \omega)$  are given by [21]

$$\frac{B'_s(H, \omega)}{B'_s(H_0, 0)} = (1 - k) \frac{3k_B T}{H_0 m_B^2} \int_0^\infty f_h(d_h) \int_0^\infty f_c(d_c) m_B(d_c) \frac{M'(H, \omega)}{M_s} dd_c dd_h + k \frac{H}{H_0} \quad (10)$$

and

$$\frac{B''_s(H, \omega)}{B''_s(H_0, 0)} = (1 - k) \frac{3k_B T}{H_0 m_B^2} \int_0^\infty f_h(d_h) \int_0^\infty f_c(d_c) m_B(d_c) \frac{M''(H, \omega)}{M_s} dd_c dd_h \quad (11)$$

with the particle saturation magnetization  $M_s$ , the field amplitude  $H_0$  and the magnetic moment  $m_B$ . The  $k$  factor accounts for the presence of small magnetic nanoparticles which follow the excitation field via the Néel mechanism with a Néel time constant  $\tau_N$  being much smaller than the Brownian time constant  $\tau_B$ .

### 3. Results

**Fig. 1** shows the measured MRX curves for the SHS-30 and the Strep SPIO particle systems. All curves are normalized to the flux density signal before the magnetizing field was switched off. For both samples, the MRX signal of the suspended sample (without analyte) decays much faster than that of the corresponding freeze-dried reference sample. This means that at least some part of the magnetic moments is blocked, i.e., that the Brownian mechanism dominates in suspensions. For the Strep SPIO sample the difference between the MRX curves on suspended and immobilized samples is less pronounced indicating that the dynamics of a bigger fraction of nanoparticles is dominated by the Néel mechanism. This is in agreement with our findings on unfunctionalized FeraSpin R samples where we demonstrated that only roughly one third of particles can follow a 10 kHz excitation via the Brownian mechanism [22]. The curves of the BNF 80 and BNF 100 samples are not shown because their behavior is in between that of the other two samples.

Clearly discernible differences between the liquid samples with and without AFP were only found for the SHS-30 samples (see **Fig. 1(a)**) since these particles are dominated by the Brownian relaxation and exhibit a small volume compared to the other samples. Néel relaxation dominated particles are not influenced by changes of the hydrodynamic size. As **Fig. 1(b)** exemplarily shows no difference in relaxation signal is observed for the multi-core

nano particle sample Strep SPIO upon binding to AFP since a significant portion of particles is dominated by the Néel mechanism. In addition, the Brownian time constant of a small particle is more affected by the growth of the hydrodynamic diameter [13]. Consequently, the change in the relaxation curve upon binding is more pronounced for the SHS-30 sample compared to samples BNF 80 and BNF 100 (data not shown). The analysis of even smaller particles and related hydrodynamic changes is limited by the measurement window of the fluxgate MRX since it is from about 400 μs (caused by the bandwidth of the fluxgate sensor) up to a few seconds. Analyzing the MRX curves of sample SHS-30 without and with bound AFP with the CMSM, mean hydrodynamic diameters of  $(47 \pm 28)$  nm and  $(76 \pm 149)$  nm (cf. **Table 1**) were obtained, respectively. The significantly larger mean diameter of the nanoparticles with bound AFP in combination with the much larger standard deviation indicates the appearance of agglomerates, presumably by cross-linking.

In **Fig. 2**, the ACS spectra measured on suspensions without and with AFP are shown for SHS-30, Strep SPIO, BNF 80 and BNF 100. The imaginary part of the samples without AFP could be adequately well fitted with Eq. (7) (solid lines in **Fig. 2**). The obtained hydrodynamic diameters are  $(48 \pm 18)$  nm for SHS-30,  $(128 \pm 42)$  nm for BNF 80,  $(179 \pm 68)$  nm for BNF 100 and  $(110 \pm 56)$  nm for Strep SPIO, i.e., somewhat larger than the values specified by the manufacturers. For comparison, from PCCS, hydrodynamic diameters of  $(52 \pm 10)$  nm,  $(103 \pm 18)$  nm,  $(136 \pm 25)$  nm and  $(86 \pm 16)$  nm were obtained for SHS-30, BNF 80, BNF 100 and Strep SPIO without AFP, respectively (cf. **Table 2**).

As expected the peak positions of the imaginary parts of the samples with bound AFP are pronouncedly shifted towards smaller frequencies due to the increased hydrodynamic diameter and thus Brownian time constant. However, it is also obvious that the size distributions became wider for all samples with AFP resulting in a decrease of the maximum value of the peak of  $\chi''$ . In addition, the spectra of the imaginary part of the samples with AFP became asymmetric with a raised low-frequency shoulder which is an indication of the formation of agglomerates. The  $\chi''$  spectra measured on the suspensions with AFP could not be well fitted with the generalized Debye model assuming a single lognormal distribution of hydrodynamic diameters.

The phase lag spectra measured for a rotating magnetic field of 1 mT amplitude are shown in **Fig. 3**. Here, the differences between multi-core and single-core particles are obvious. The suspension of the single-core particles SHS-30 without AFP exhibits a monotonous increase of the phase lag with increasing frequency (see **Fig. 3(a)**), which is in agreement with [13]. The conjugation of the

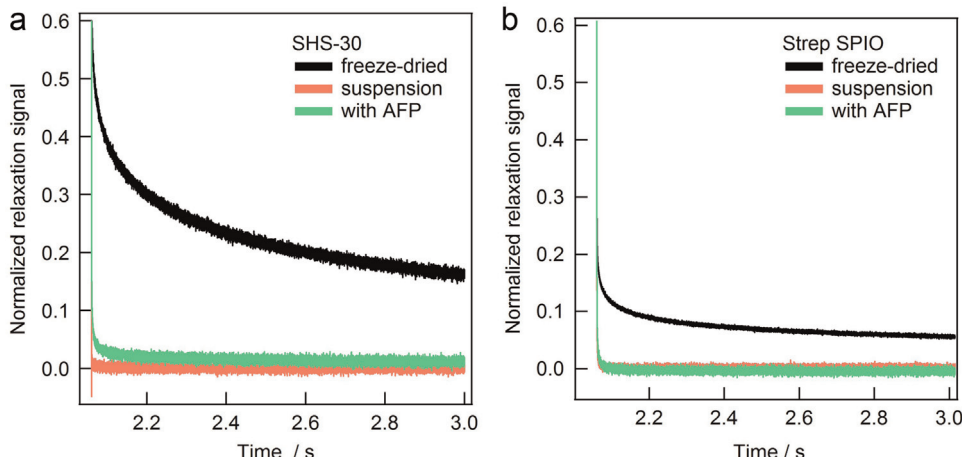


**Fig. 1.** Normalized MRX curves measured on samples (a) SHS-30 and (b) Strep SPIO. For both particle systems, measurements were performed on freeze-dried samples as well as on suspensions with and without bound AFP.

**Table 1**  
Hydrodynamic diameters of sample SHS-30 in nm.

Type	PCCS	ACS	RMF	MRX
without AFP	52 ± 10	48 ± 18	48 ± 15	47 ± 28
with AFP	103 ± 19	78 ± 70	66 ± 26	76 ± 149

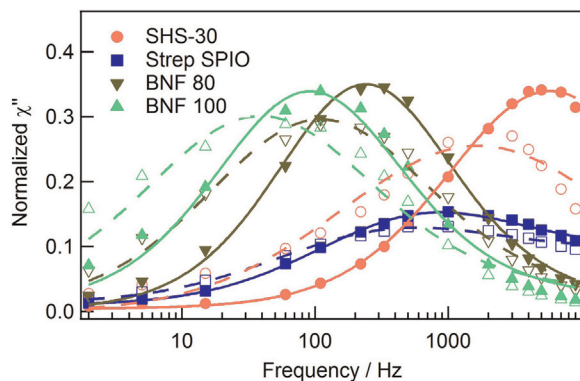


**Fig. 2.** Measured ACS spectra of samples SHS-30, Strep SPIO, BNF 80 and BNF 100 in suspension without (filled symbols) and with AFP (open symbols). Lines show fits with generalized Debye model.

**Table 2**  
Hydrodynamic diameters in nm determined by ACS and PCCS.

	SHS-30	BNF 80	BNF 100	Strep SPIO
ACS	48 ± 18	128 ± 42	179 ± 68	110 ± 56
PCCS	52 ± 10	103 ± 18	136 ± 25	86 ± 16

nanoparticles with AFP causes a clear phase lag rise over the whole frequency range. On the other hand, the phase lag spectra measured on the multi-core samples show a steep increase at low frequencies followed by a constant phase lag at around 15° for Strep SPIO or even a decrease at higher frequencies for BNF 100 and BNF 80. The phase lag spectrum of BNF 80 is qualitatively similar to that of BNF 100 except that the initial phase lag rise is somewhat shallower as a consequence of the smaller hydrodynamic diameter. The decrease at higher frequencies can be explained by a large fraction of nanoparticles which follow the rotating field via the Néel mechanism. To illustrate this, Fig. 3(b) shows the phase lag difference  $\Delta\varphi$  between the phase

lags measured on bound and unbound samples vs. frequency. The curve of the SHS-30 samples shows a maximum at 2.5 kHz with a phase lag change of 12°, which is in qualitative agreement with measurement results regarding the binding of protein G functionalized nanoparticles to IgG [13]. In contrast, the phase lag change for samples BNF 80 and BNF 100 exhibits a positive value only at frequencies below 200 Hz and it becomes negative at higher frequencies. The phase lag change of the Strep SPIO samples exhibits a similar behavior, except that the effect is smaller than observed for BNF 100 due to the higher fraction of nanoparticles which follow the rotating field via the Néel mechanism with a very short time constant  $\tau_N$ . Such particles can follow the excitation field almost instantaneously, i.e., without a significant phase lag.

**Table 2** summarizes the hydrodynamic diameters of single-core nanoparticle samples SHS-30 obtained from PCCS, ACS, RMF and MRX measurements. For all techniques, the hydrodynamic diameters of the unbound nanoparticles are in good agreement to each other. The hydrodynamic diameter of the sample with bound AFP shows an increase of the mean value but also a significantly wider distribution indicating the formation of aggregates. The mean value of the order of 75 nm by far exceeds what would be expected for a nanoparticle coverage with a single layer of AFP. Due to their multivalency, streptavidin functionalized nanoparticles and biotinylated analytes can cross-link, thus forming larger aggregates of nanoparticle-analyte complexes. This formation of aggregates also manifests itself in the asymmetric spectrum of the imaginary part of the ac susceptibility (cf. Fig. 2). Apparently, the chosen ratio between biotinylated proteins and streptavidin functionalized nanoparticles was sufficiently large to cause cross-linking. Whereas the ACS and RMF techniques turn out to be capable of detecting small analytes such as proteins even without such cross-linking, due to the measurement window from typically 400 μs to a few seconds MRX is powerful for the detection of larger analytes, such as bacteria, or for the realization of agglutination assays which are based on cross-linking [2].

For the multi-core particle systems, the situation is more complex. Although the mean hydrodynamic diameter of Strep SPIO is smaller than those of the BNF samples, the change of the susceptibility spectrum and of the phase lag in a RMF measurement upon binding of AFP is comparably small. This is caused by the large fraction of nanoparticles which follow the magnetic excitation via the Néel mechanism. In addition, the phase lag change spectrum upon binding of AFP shows a crossing from positive values – as observed for the SHS-30 single-core nanoparticles over the whole frequency range – at low frequencies to negative values.

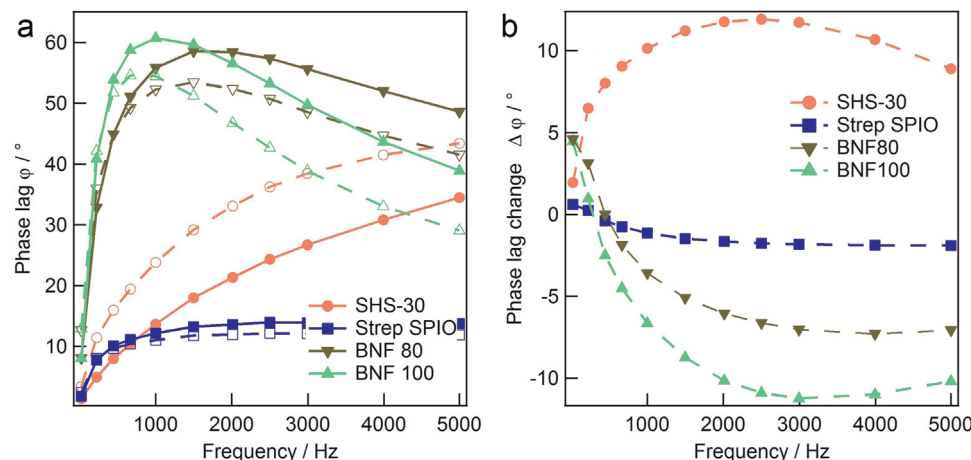


**Fig. 3.** (a) Measured phase lag spectra for 1 mT rotating magnetic field of samples SHS-30, Strep SPIO, BNF 80 and BNF 100 in suspension without (filled symbols and solid lines) and with conjugated AFP (blank symbols and dashed lines). (b) Phase lag change upon binding of AFP. The change from positive to negative phase lag change values illustrates the crossing of the phase lag spectra observed in (a).

This behavior can be explained by an increase of the Brownian time constant in conjunction with the coexistence of Néel particles. In addition, the increase of the hydrodynamic size can cause a transition from Brownian to Néel relaxation dominated particles resulting in a negative sign of the phase lag change. This effect is especially supported by cross-linking. One should note that the spectra of the imaginary part of the ac susceptibility behave – at least on a first glance – as expected, i.e., the conjugation of analytes causes a shift of the maximum of  $\chi''$  to lower frequencies.

For the realization of homogenous bioassays with the RMF technique, the single-core particles SHS-30 turned out to be more suitable than the multi-core particles. The maximum phase lag change of  $+12^\circ$  by far exceeds the values obtained for the other particle systems (see Fig. 3(b)). For the multi-core particles Strep SPIO, the high fraction of nanoparticles which follow the excitation field via the Néel mechanism causes only minor changes (maximum of  $+2^\circ$ ) of the phase lag upon binding of analytes. The maximum phase lag change of the BNF 100 sample is with a value of  $-11^\circ$  similarly high as for the SHS-30 sample but with a negative sign. Whether this negative phase lag change maximum can be used for a quantification of analytes, needs to be investigated by analyte concentration dependent measurements.

In the ACS measurements, the largest relative shift of the spectra was observed for the SHS-30 sample which is a consequence of the MNP's smaller hydrodynamic diameter compared to the multi-core particle systems BNF 80 and BNF 100. In contrast, a shift of the maximum in the imaginary part of the ACS is hardly discernable for the Strep SPIO samples. Again, this is caused by the large fraction of nanoparticles which follow the excitation field via the internal Néel mechanism. For both measurement techniques, ACS and RMF, the effects would be more pronounced if larger magnetic field amplitudes were applied which is a consequence of the magnetic-field dependence of the Brownian time constant [23].

#### 4. Conclusion

In summary, we have compared homogeneous bioassays, binding AFP to different streptavidin-functionalized single- and multi-core nanoparticle systems utilizing different dynamic magnetic measurement techniques. Since all applied techniques are based on detecting changes in hydrodynamic size, it is vitally important that the dynamics of the majority of nanoparticles is dominated by the Brownian mechanism. Single-core MNPs with large magnetic moments and small hydrodynamic diameters turned out to be most suitable. Both ACS and RMF measurements are well suited for the detection of small analytes. The phase lag change upon binding measured when the MNPs are exposed to a rotating magnetic field was found to exhibit a rather complex behavior for multi-core MNP systems. MRX was found to be suitable for the detection of small analytes such as proteins if cross-linking is present.

#### Acknowledgements

Financial support by the European Commission Framework Programme 7 under the NAMDIATREAM project (NMP-2010-246479) is gratefully acknowledged.

#### References

- [1] W. Weitschies, R. Kötitz, T. Bunte, L. Trahms, Determination of relaxing or remanent nanoparticle magnetization provides a novel binding-specific technique for the evaluation of immunoassays, *Pharm. Pharmacol. Lett.* 7 (1997) 1–4.
- [2] D. Eberbeck, F. Wiekhorst, U. Steinhoff, et al., Quantification of biomolecule agglutination by magnetorelaxometry, *Appl. Phys. Lett.* 95 (2009) 213701.
- [3] H.L. Grossman, W.R. Myers, V.J. Vreeland, et al., Detection of bacteria in suspension by using a superconducting quantum interference device, *Nat. Acad. Sci. U. S. A.* 101 (2004) 129–134.
- [4] E. Heim, F. Ludwig, M. Schilling, Binding assays with streptavidin-functionalized superparamagnetic nanoparticles and biotinylated analytes using fluxgate magnetorelaxometry, *J. Magn. Magn. Mater.* 321 (2009) 1628–1631.
- [5] A.P. Astalan, F. Ahrentorp, C. Johansson, et al., Biomolecular reactions studied using changes in Brownian rotation dynamics of magnetic particles, *Biosens. Bioelectron.* 19 (2004) 945–951.
- [6] S.H. Chung, A. Hoffmann, S.D. Bader, et al., Biological sensors based on Brownian relaxation of magnetic nanoparticles, *Appl. Phys. Lett.* 85 (2004) 2971.
- [7] K. Enpuku, Y. Tamai, T. Mitake, et al., ac susceptibility measurement of magnetic markers in suspension for liquid phase immunoassay, *J. Appl. Phys.* 108 (2010) 034701.
- [8] C.-Y. Hong, C.C. Wu, Y.C. Chiu, et al., Magnetic susceptibility reduction method for magnetically labeled immunoassay, *Appl. Phys. Lett.* 88 (2006) 212512.
- [9] C.C. Yang, S.Y. Yang, H.H. Chen, et al., Effect of molecule-particle binding on the reduction in the mixed-frequency alternating current magnetic susceptibility of magnetic bio-reagents, *J. Appl. Phys.* 112 (2012) 024704.
- [10] H.-J. Krause, N. Wolters, Y. Zhang, et al., Magnetic particle detection by frequency mixing for immunoassay applications, *J. Magn. Magn. Mater.* 311 (2007) 436–444.
- [11] P.I. Nikitin, P.M. Vetroshko, T.I. Ksenovich, New type of biosensor based on magnetic nanoparticle detection, *J. Magn. Magn. Mater.* 311 (2007) 445–449.
- [12] L. Tu, Y. Jing, Y. Li, et al., Real-time measurement of Brownian relaxation of magnetic nanoparticles by a mixing-frequency method, *Appl. Phys. Lett.* 98 (2011) 213702.
- [13] J. Dieckhoff, A. Lak, M. Schilling, et al., Protein detection with magnetic nanoparticles in a rotating magnetic field, *J. Appl. Phys.* 115 (2014) 024701.
- [14] J. Dieckhoff, M. Schilling, F. Ludwig, Magnetic marker based homogeneous bioassays utilizing rotating magnetic fields, *J. Appl. Phys.* 115 (2014) 17B304.
- [15] D. Eberbeck, F. Wiekhorst, U. Steinhoff, et al., Aggregation behaviour of magnetic nanoparticle suspensions investigated by magnetorelaxometry, *J. Phys.: Cond. Mater.* 18 (2006) S2829–S2846.
- [16] F. Ludwig, E. Heim, M. Schilling, et al., Characterization of superparamagnetic Fe<sub>3</sub>O<sub>4</sub> nanoparticles by fluxgate magnetorelaxometry for use in biomedical applications, *J. Appl. Phys.* 103 (2008) 07A314.
- [17] F. Ludwig, E. Heim, M. Schilling, Characterization of superparamagnetic nanoparticles by analyzing the magnetization and relaxation dynamics using fluxgate magnetometers, *J. Appl. Phys.* 101 (2007) 113909.
- [18] S.H. Chung, A. Hoffmann, K. Guslienko, et al., Biological sensing with magnetic nanoparticles using Brownian relaxation (invited), *J. Appl. Phys.* 97 (2005) 10R101.
- [19] F. Ludwig, Characterization of magnetic core–shell nanoparticle suspensions using ac susceptibility for frequencies up to 1 MHz, *AIP Conf. Proc.* 1311 (2010) 249–254.
- [20] J. Dieckhoff, M. Schilling, F. Ludwig, Fluxgate based detection of magnetic nanoparticle dynamics in a rotating magnetic field, *Appl. Phys. Lett.* 99 (2011) 112501.
- [21] T. Yoshida, K. Enpuku, J. Dieckhoff, et al., Magnetic fluid dynamics in a rotating magnetic field, *J. Appl. Phys.* 111 (2012) 053901.
- [22] F. Ludwig, T. Wawrzik, T. Yoshida, et al., Optimization of magnetic nanoparticles for magnetic particle imaging, *IEEE Trans. Magn.* 48 (2012) 3780–3783.
- [23] J. Dieckhoff, T. Yoshida, K. Enpuku, et al., Homogeneous bioassays based on the manipulation of magnetic nanoparticles by rotating and alternating magnetic fields, *IEEE Trans. Magn.* 48 (2012) 3792–3795.